Benavente Martínez, R.; Pruna, AI.; Borrell Tomás, MA.; Salvador Moya, MD.; Pullini, D.; Penaranda-Foix, FL.; Busquets Mataix, DJ. (2015). Fast route to obtain Al2O3-based nanocomposites employing graphene oxide: Synthesis and Sintering. Materials Research Bulletin. 64:245-251. doi:10.1016/j.materresbull.2014.12.075.

Fast route to obtain Al_2O_3-based nanocomposites employing graphene oxide: synthesis and sintering

R. Benavente[1], A. Pruna[1,2]*, A. Borrell[1], M. D. Salvador[1], D. Pulini[3], F. Peñaranda-Foix[4], D. Busquets[1]

[1]Instituto de Tecnología de Materiales, Universitat Politècnica de València, Camino de Vera, s/n, 46022 Valencia, Spain

[2]University of Bucharest, 405 Atomistilor, 077125 Bucharest, Romania

[3]Fiat Research Centre, 50 Torino Street, 10043 Orbassano, Italy

[4] Instituto de Aplicaciones de las Tecnologías de la Información y de las Comunicaciones Avanzadas (ITACA), Universidad Politécnica de Valencia, Camino de Vera s/n, 46022, Valencia, Spain

*Corresponding author. E-mail address: apruna@itm.upv.es. Tel.: +34 627018518

Graphical abstract

FE-SEM images of fracture surfaces of the sintered **composites**: (a) conventional and (b) microwave technique.

Highlights

- *Ultrasonication and freeze drying were used to disperse GO into Al_2O_3 matrix.*
- *Al_2O_3-**rGO powders** were densified by conventional and microwave sintering.*
- *Microwave technology resulted in smaller grain size than conventional one.*

- *Presence of rGO in the composites resulted in improved electrical properties.*

Abstract

A fast approach based on microwave technology was employed for the sintering of novel composites of alumina and using graphene oxide (GO) as susceptor. The thermal stability and structure of GO materials produced by chemical oxidation of graphite were characterized. The morphology, structure and mechanical properties of the composites sintered by microwave approach were reported to the counterparts sintered by conventional method. The results indicated the formation of an inter-connecting graphene network promoted the electrical conductivity in the composite having only 2 wt.% GO. Hardness and elastic modulus decreased significantly in samples sintered by conventional method due to lower values of density while microwave technology allowed to achieve a positive effect on the densification and showed a smaller grain size when compared to the one achieved by conventional heating.

Keywords: A. Composites; B. Mechanical properties; C. Electron microscopy; C. Raman spectroscopy; D. Electrical properties.

1. INTRODUCTION

Graphene had evolved as a promising alternative to carbon nanotubes (CNTs) and great interest has been devoted to its research not only from fundamental point of view but also device applicability [1-6]. Thanks to its unique combination of electrical, mechanical and thermal [2, 7, 8] properties, graphene is considered an ideal second phase in order to improve simultaneously the

mechanical, electrical and thermal properties of metals, polymers and ceramics [9-12].

Alumina is one of the highly used structural ceramics in the materials industry having various potential applications including high speed cutting tools, dental implants, chemical and electrical insulators, wear resistance parts and coatings thanks to the hardness, chemical inertness and high electrical and thermal insulation properties [13-16]. However, the field of applications is significantly restricted by brittleness and fabrication difficulties.

In this respect, it was shown that carbon materials are very good microwave absorbers, i.e., they are easily heated by microwave radiation [17]. Under exposure to microwave heating they are subjected to transformations giving rise to new carbon materials with tailored properties, that can be further used as microwave receptors in order to allow other materials which are transparent to microwaves, i.e., alumina, to heat indirectly. The main advantage of microwave over the traditional heating techniques is based on the different mechanism involved in heating carbons which results into: (i) a considerable decrease in the time scale, which in most cases implies a smaller consumption of energy; (ii) a reduction in the number of steps involved in the global process, eliminating the need for other reagents, devices, etc. and (iii) an increase in the efficiency of the global process. These advantages translate into a more economically competitive final product.

The aim of this work is to demonstrate the successful obtainment of alumina composites by employing microwave sintering approach and graphene oxide (GO) as microwave receptor. To the best of our knowledge, this is the first report on such novel composites sintered by microwave technology. Simple and

fast modified Hummers method was shown to produce controllable good quality graphene oxide (GO) flakes [18]. Large scalability and homogeneous distribution of graphene sheets are the main requisites of the increasingly researched graphene-based composites for which the conversion of GO can be taken into consideration thanks to the major advantage of material availability at low cost and efficient bulk production. Here, the GO materials were dispersed together with Al_2O_3 powder to produce a homogeneous mixture by using simple sonication treatment and freeze drying. The thermal reduction of GO took place during the sintering of Al_2O_3-GO composites when the oxygen-containing functional groups introduced on both the edge and basal plane of the nanosheets by oxidation of graphite are removed, resulting in reduced GO (rGO) with aromatic graphene network partially restored. Among the reduction methods, thermal treatment was found to be one of the most effective [19]. The temperature and duration applied in the sintering procedure were sufficiently high and short enough to avoid additional reduction procedures and prevent the denaturation of graphene network. The effect of GO addition on the structure, morphology, electrical and mechanical properties of the ceramic composites sintered by microwave approach was reported to the counterparts sintered by conventional method.

2. EXPERIMENTAL PROCEDURE

2.1. Graphene oxide (GO) preparation

Modified Hummer's method was applied for the synthesis of graphene oxide, as Pruna et al. described previously [18]. Basically, natural graphite powder 200 mesh (99.9995%, Alfa Aesar) was oxidized for 2 h in a 150 mL mix of H_2SO_4:H_3PO_4 (6:1 v/v) and 6 g $KMnO_4$. The mixture was cooled to room

temperature, diluted with deionized water and 30% H_2O_2 was added. Further, the mixture was filtered and purified with HCl and washed with deionized water till neutral pH was reached. The obtained product was subjected to a drying process at 50 ºC for 24 h.

2.2. Powder mixture preparation

In order to prepare uniform and well dispersed nano-composites we used a powder processing route. The obtained GO was added in deionized water and then sonicated for 30 min in an ultrasonic probe (UP 400 S, Hielscher, Stuttgart, Germany). After sonication, the appropriate amount of commercially available α-Al_2O_3 powder (Taimei TM-DAR Chemicals Co. Ltd, Japan, particle size-150 nm, specific surface area-14.5 m^2/g and purity-99.99%) was added to the prepared suspension using magnetic stirring and the mixture was subjected to sonication for another 10 min. The final suspension was frozen in a liquid nitrogen bath and then dried in a freeze drier (Cryodos-50, Telstar, Spain) for 24 h. The dried powder mixture was ground and sieved using 60 mesh.

2.3. Al_2O_3-GO powder sintering

Al_2O_3-GO nanocomposites with 2 wt.% loading were sintered under vacuum using two techniques: a conventional furnace at 1400 ºC for a dwell time of 2 h and a heating rate of 10 ºC/min and, a non-conventional sintering as microwave technology at 1400 ºC without susceptor using the heating rate of 200 ºC/min with 10-min of holding time at the maximum temperature. The temperature of the sample is monitored by an infrared radiation thermometer (Optris CT-Laser LT, 8-14 μm), which is focused on the test sample via the small circular aperture in the wall of the test cell [20].

2.4. Characterization methods

GO characterization

Absorbance ultraviolet-visible (UV-Vis) spectra were recorded with a Lambda 35 (Perkin Elmer) spectrophotometer. Thermogravimetric analysis (TGA) was conducted with a Q50 (TA Instruments) thermal analyser under nitrogen flow at a scanning rate of 10 ºC/min. The FTIR (Fourier Transform Infrared Spectrometer) spectra were acquired on a Perkin Elmer FTIR Spectrum BX spectrometer in ATR mode. The crystalline phases present were determined by X-ray diffraction (XRD, D2 Phaser, Bruker, Germany) using Cu Kα radiation and a voltage of 30 kV. The scan range (2θ) was from 5º to 50º with a step size of 0.02º. The recording step time was 0.3 s. Raman spectra were acquired on inVia Renishaw spectrometer with 514.5 nm wavelength of incident laser light. Atomic Force Microscope (AFM) (Bruker, Germany) was used to obtain micrographs operating in tapping mode. The investigation of the morphology has been performed by Transmission Electron Microscopy (TEM, TECNAI-10, Philips).

The measurement for carbon content in GO was performed by combustion of 1 mg GO sample at 1050 ºC (LECO CHNS-932). Under these conditions carbon material is transformed into CO_2, H_2O and possibly SO_2 where sulphur content remained in GO material from the oxidant used in modified Hummers procedure. The obtained values indicated the necessity of further purification procedure where relevant. These three compounds were detected and evaluated for its absorption in the infrared spectrum. Nitrogen formed NO_X, subsequently reduced to N_2 with Cu, this species being quantified by gas chromatography from the signal obtained with a thermal conductivity detector

(TCD). Thus, the percentage of carbon, hydrogen, nitrogen and sulphur in each of the samples were calculated.

The oxygen content was determined by graphite furnace coupled at LECO VTF 900 equipment. 1 mg of sample was pyrolyzed to 1350 ºC under a helium flow of 225 ml min^{-1}. The generated CO got oxidized to CO_2 forming CuO, which was evaluated and thereby obtaining the oxygen content of the sample directly.

Composite characterization

The bulk density of the samples was measured by the Archimedes method (ASTM C373-88) with ethanol as the immersion medium using densities of 3.98 and 2.0 g/m^3 for Al_2O_3 and GO, respectively. The relative density was calculated by dividing the bulk density with the theoretical density of the powder mixture.

Nanomechanical properties such as hardness and Young's modulus of samples were obtained by nanoindentation technique (Model G200, MTS Company, USA). The sintered samples were previously cut longitudinally in half cylinders with a diamond saw and polished (Struers, model RotoPol-31) with 0.25 µm diamond paste. To carry out indentations at very low depths, a Berkovich diamond tip was used with radius less than 20 nm. In order to ensure the quality of the tip throughout the work, pre- and post- calibration procedures were performed for this indenter ensuring the correct calibration of its function area and correct machine compliance. The nanomechanical properties of the Al_2O_3-rGO ceramics were evaluated from the load-displacement nanoindentation data using the widely accepted Oliver and Pharr model [21].

The fracture surface sections of the sintered samples have been observed using a field emission gun scanning electron microscope (FE-SEM, HITACHI S-

4800, SCSIE of the University of Valencia). Four-point probe measurements were performed for the electrical properties.

3. RESULTS AND DISCUSSION

3.1. Characterization of GO

Figure 1a shows the typical FTIR spectra of as-synthesized GO material. With respect to the characteristics exhibited by parent graphite, the spectrum of GO confirmed the successful oxidation of graphite by the appearance of peaks at 1744, 1518, 1234, 1128 and 1068 cm^{-1} attributed to oxygen functional groups namely carbonyl, carboxyl, hydroxyl and epoxy [18]. On the other hand, the peak corresponding to graphitic domains at 1645 cm^{-1} can be still observed in GO indicating the presence of un-oxidized material. The broad band at 3000-3500 cm^{-1} in GO was attributed to adsorbed water [22].

XRD was further performed in order to estimate the oxidation degree and according to the spectra in figure 1b, it was found that the typical (002) diffraction peak of graphite was down-shifted from 26.5 degrees to 11.5 degrees confirming the successful expansion of graphite due to the intercalating functional groups as the interlayer spacing changed from 0.35 to 0.68 nm upon oxidation. Moreover, the UV-Vis spectroscopy results confirmed these findings as the spectra recorded for the aqueous dispersion of GO material exhibited the typical absorption peak at 225 nm attributed to π-π^* transitions of aromatic C=C bonds and a shoulder peak at about 300 nm attributed to n-π^* transitions of C=O bonds [23] (see figure 1 in supplementary file).

The thermal behaviour of GO was studied by TG analysis and it was observed that GO exhibited much lower thermal stability than graphite with various step-wise losses attributed to the adsorbed water (around 10% loss at 100°C), labile

oxygen groups (a steep loss was observed at about 200°C followed by a steady trend till 500°C) and the removal of more stable ones (an increased weight loss of about 45% was registered at 600°C), respectively (see figure 2 in supplementary file). The obtained results confirmed earlier findings that overall amount of oxygen functionalities, their type and distribution in the GO materials can be tailored by appropriate graphite oxidation parameters [24].

The morphology of as-prepared GO was characterized by TEM and AFM as shown in figure 2. The TEM image in figure 2a depicts the GO as large transparent folded sheets resembling silk veil waves while AFM characterization revealed GO sheets with an average thickness of folded sheets of around 2 nm while the lateral size ranged from hundreds nanometres to few microns. GO folded sheets are expected to be “thicker” than graphene due to the presence of covalently bonded oxygen and the displacement of the sp^3-hybridized carbon atoms slightly above and below the original graphene plane.

3.2. Characterization of sintered Al_2O_3-rGO composites

Table 1 shows the analysis for carbon content, bulk densities and electrical resistivity of the prepared composites as a function of sintering process. The graphene content of the composites were found in similar percentage. This indicated that in the mixture and after densification by two methods, the carbon content remain similar.

Fully dense composites were obtained by microwave (MW) with a dwell time of 10 min, thus limiting the damage induced in rGO by prolonged exposure at high temperature. As a result of the transformation of GO into rGO during the sintering, the addition of even very small amounts of GO to the alumina matrix resulted into an electrically conductive composite fact that confirms the

successful dispersion of GO into the alumina matrix and reduction of GO. This value indicates the exponential increase of the conductivity up to 11 orders of magnitude in comparison to the monolithic alumina (10^9 Ω cm). Centeno et al. [12] found that the percolation threshold of the Al_2O_3/graphene composites was found around 0.22 wt.% of graphene (~50 Ω cm).

The value of electrical resistivity obtained (0.39 Ω cm) for Al_2O_3-rGO sintered by microwave, is good enough to be able to shape the nanocomposite using the electro discharge machining (EDM) technique while the value obtained for conventional sintering (CS) is similar to the one reported for GO reduced by both hydrazine and thermal treatments at 400 and 1100 °C in vacuum [25]. The improvement of the electrical properties due to heat treatment has been attributed to mechanisms such as restoration of sp^2 C–C bonds and cross-linking between reduced GO sheets during the thermal annealing process [25]. This technique can be an effective alternative for manufacturing complex shape components from hard materials but certain electrical conductivity (>0.3-1 S m^{-1}) is required. Previous studies have shown that EDM can be successfully applied to machine ceramic materials, including single-phase ceramics and ceramic/ceramic and metal/ceramic composites if the electrical resistivity was below 100 Ω cm [26, 27]. Attempts have also been reported to increase the electrical conductivity of ceramic materials in order to make them suitable for EDM operation [28]. Among these ceramic materials, Al_2O_3 is a very interesting material for technological applications. However, due to its insulator character it requires electrical conductivity in order to be shaped using EDM.

Raman spectroscopy was used to confirm the structural integrity of the graphene in the alumina matrix upon sintering process (figure 3a). The two

main Raman features arising from the first-order scattering of the E_{2g} phonon of sp^2 C atoms and the breathing mode of k-point photons of A_{1g} symmetry, respectively [29] were observed for all samples. The effects of the reduction of GO during the sintering approaches on the Raman characteristics show that both D and G bands undergo significant changes and confirm the successful reduction of GO by the sintering approaches of alumina composites. Specifically, the I_D/I_G ratio increased upon microwave reduction procedure indicating a disorder enhancement [30] while the reduction of GO upon CS of composites resulted in a lower I_D/I_G ratio which is indicative of a defect healing effect of CS (see table 2). Moreover, this effect is confirmed by the red-shift of the G band position of rGO obtained upon reduction by CS, as well. The red shift of the G band was attributed to tensile strain weakening the bond and thus lowering the vibration frequency due to the elongation of C-C bonds [31]. Additionally, two small peaks were observed for all rGO materials: a 2D band sensitive to the aromatic C-structure at around 2695 cm^{-1} and an additional peak at 2945 cm^{-1} ascribed to the G + D combination mode induced by disorder or the D + D' band [32]. The rGO material obtained by CS exhibited higher I_{2D}/I_G values than by microwave approach with respect to parent GO, thus indicating better restoration of aromatic carbon structure by thermal treatment by CS technique than by MW approach, in good agreement with previous research results on sintering of alumina-graphene composites [11]. The observed result could be explained by a healing process thanks to carbon radicals introduced while thermally reducing the GO in CS [33]. On the other hand, the intensity ratio I_{2D}/I_G is sensitive to doping [34] and it is highly affected by the sintering technique, that is, it decreases with the annealing during MW procedure, while

for CS approach it increases. Thermal treatments at 1100 °C in vacuum have been previously reported to yield a significantly reduced GO [35]. Further investigation is ongoing to identify the chemistry of the GO sheets under the various annealing conditions employed during the sintering approaches applied in this work.

The XRD spectra in figure 3b show the crystal system of the hexagonal α-Al_2O_3 ceramics (JCPDS #82-1468). Similar pattern was detected upon conventional sintering for pure Al_2O_3 specimens with a marked decrease in the full width at half maximum (FWHM), indicating an increase in the crystallite size. On the contrary, the microwave technology resulted in a FWHM value close to the parent powder. The presence of GO in the powder mix was indicated by a low broad shoulder due to the low content in the composite. Upon sintering, the rGO presence was indicated by the shift of the corresponding peak to higher degrees (about 22°) as depending on the reduction produced during the applied thermal treatment. A small difference in the (002) peak position for rGO and the corresponding FWHM indicated that the reduction of GO is affected by the thermal treatment applied. No detectable second phase was revealed indicating the absence of significant reaction between GO and alumina.

The microstructure of sintered ceramic samples was examined. In order to evaluate the effect of sintering method and the distribution of GO/rGO in the composites, fracture surfaces were investigated, as depicted in figure 4. The FE-SEM images of the samples sintered by conventional and microwave sintering were compared to those of the pure Al_2O_3 and Al_2O_3-GO powders. The Al_2O_3 subjected to conventional sintering presented a fully-dense structure of mainly intergranular fracture mode (see figure 4c) with uneven grains (the

average grain size reaches about 475 nm). It is clearly seen that conventional sintering resulted in a marked increase of grain size with respect to the un-sintered powder. By comparing the composite obtained by conventional sintering in figure 4d with the pure Al_2O_3 in figure 4c it is observed that the presence of GO doesn't result in obvious change in grain size indicating that the small grain size observed in figure 4e (grain size of 180 nm) is due to the microwave technology, in agreement with the XRD results. The counterparts obtained by MW exhibited an increase in the uniformity. When heating materials with microwave energy, the sintering occurs due to a self-heating of the material and the maximum temperature is found in the core of the material. Therefore, the most energetic area is located within grain centre. Consequently, the grain boundary diffusion and subsequent formation of sintering neck is less favoured. This effect can lead directly to the second stage of the sintering process, densification and microstructural change [36], skipping the first phase, which causes the neck between grains and thickening.

As depicted in figure 4 b, it is observed the Al_2O_3 grains decorate the GO sheets in the powder mix due to the presence of residual oxygen functional groups in GO. The increase in the GO folding could be attributed to the freeze-drying procedure. These observations indicate the dispersion of the GO flakes in the ceramic matrix is size-dependent. The rGO in the sintered composites appear trapped in between the grain boundaries (see arrows in figure 4d and e) that could prevent migration of grain boundaries and result in a refining of microstructure. Their size is clearly decreased in the case of microwave approach and is attributed to the defects introduced by microwave heating and non-homogeneous reduction. The pulled-out sheets dispersed in the matrix and

the poor distribution could be explained by the shearing stress the thinner sheets were subjected to while the thicker ones exposed themselves in the fracture.

The evolution of the hardness (*H*) and Young's modulus (*E*) with penetration depth for studied materials is plotted in figure 5. A common trend can be clearly detected in the behaviour of *H* and *E* values as a function of penetration depth. Hardness and Young's modulus values decrease when penetration depth increases. The slope of the curves is very slow and they finally stabilize in all experimented penetration depths. Dispersion of *H* and *E* are very large for the initial 200 nm of penetration depth. This fact could be due to the implicit experimental variability of factors such as tip-sample interactions, sample roughness and tip rounding [37]. The slight decrease of *H* with penetration depth could be due to the indentation size effect [38]. Concerning elastic modulus, the obtained values show a little decrease according to the penetration depth. In addition, the higher is the depth of penetration, the more likely is that residual porosity and grain boundaries can affect *H* and *E* values. Hardness and elastic modulus values for Al_2O_3-rGO bulk materials sintered by microwave technology are reported for the first time. Microwave sintered Al_2O_3-rGO materials exhibited superior mechanical properties values when compared with conventional fired materials, as was expected from their higher densities.

4. CONCLUSIONS

Novel Al_2O_3-rGO composites were densified (~99%) by using non-conventional microwave technology at 1400 ºC. Reduction of GO took place simultaneously with the densification process and resulted in few-layers rGO sheets. The grain size of Al_2O_3 matrix and the mechanical properties of the composites were

markedly affected by the sintering method while the presence of rGO was indicated to improve the electrical properties. The results of this work indicate the high potential of rGO and microwave technology to suit various engineering applications of ceramic composites.

Acknowledgments Financial support from European Commission (project no. NMP3-SL-2010-246073), Universidad Politécnica de Valencia (project SP20120677) and Ministerio de Economía y Competitividad – MINECO (project TEC2012-37532-C02-01, co-funded by ERDF (European Regional Development Funds) is gratefully acknowledged. A.B. acknowledges the Spanish Ministry of Science and Innovation (contract JCI-2011-10498). A.P. acknowledges support from Romanian Authority for Scientific Research – UEFISCDI (project no. PN-II-RU-PD-2012-3-0124).

References

[1] Wu JS, Pisula W, Mullen K. Graphenes as potential material for electronics. Chem Rev 2007;107:718-747.

[2] Geim AK, Novoselov KS. The rise of graphene. Nat Mater 2007;6(3):183-191.

[3] Liao L, Lin YC, Bao MQ, Cheng R, Bai JW, Liu YA, Qu YQ, Wang KL, Huang Y, Duan XF. High-speed graphene transistors with a self-aligned nanowire gate. Nature 2010;467(7313):305-308.

[4] Pasanen P, Voutilainen M, Helle M, Song XF, Hakonen PJ. Graphene for future electronics. Phys Scripta 2012;T146:014025.

[5] Tapaszto O, Tapaszto L, Marko M, Kern F, Gadow R, Balazsi C. Dispersion patterns of graphene and carbon nanotubes in ceramic matrix composites. Chem Phys Lett 2011;511(4-6):340-343.

[6] Carrera-Cerritos R, Baglio V, Aricò AS, Ledesma-García J, Sgroi MF, Pullini D, Pruna AJ, Mataix DB, Fuentes-Ramírez R, Arriaga LG. Improved Pd electro-catalysis for oxygen reduction reaction in direct methanol fuel cell by reduced graphene oxide. Appl Catal B-Environ 2014;144:554-560.

[7] Lee C, Wei XD, Kysar JW, Hone J. Measurement of the elastic properties and intrinsic strength of monolayer graphene. Science 2008;321(5887):385-8.

[8] Balandin AA, Ghosh S, Bao WZ, Calizo I, Teweldebrhan D, Miao F, Lau CN. Superior thermal conductivity of single-layer graphene. Nano Lett 2008;8(3):902-7.

[9] Liu MC, Chen CL, Hu J, Wu XL, Wang XK. Synthesis of magnetite/graphene oxide composite and application for cobalt (II) removal. J Phys Chem C 2011;115(51):25234-40.

[10] Kuilla T, Bhadra S, Yao DH, Kim NH, Bose S, Lee JH. Recent advances in graphene based polymer composites. Prog Polym Sci 2010;35(11):1350-75.

[11] Centeno A, Rocha VG, Alonso B, Fernández A, Gutierrez-Gonzalez CF, Torrecillas R, Zurutuza A. Graphene for tough and electroconductive alumina ceramics. J Eur Ceram Soc 2013;33:3201-3210.

[12] Cembrero J, Pruna A, Pullini D, Busquets-Mataix D. Effect of combined chemical and electrochemical reduction of graphene oxide on morphology and structure of electrodeposited ZnO. Ceramics Intl 2014;40 (7): 10351–10357.

[13] Ahmad I, Cao HZ, Chen HH, Zhao H, Kennedy A, Zhu YQ. Carbon nanotube toughened aluminium oxide nanocomposite. J Eur Ceram Soc

2010;30(4):865-873.

[14] Borrell A, Rocha VG, Torrecillas R, Fernández A. Surface coating on carbon nanofibers with alumina precursor by different synthesis routes. Compos Sci Technol 2011;71(1):18-22.

[15] Borrell A, Rocha VG, Torrecillas R, Fernández A. Improvement of CNFs/ZrO_2 composites properties with a zirconia nanocoating on carbon nanofibers by sol-gel method. J Am Ceram Soc 2011;94(7):2048-2052.

[16] Tang DX, Lim HB, Lee KJ, Lee CH, Cho WS. Evaluation of mechanical reliability of zirconia-toughened alumina composites for dental implants. Ceram Int 2012;38(3):2429-2436.

[17] Menéndez JA, Arenillas A, Fidalgo B, Fernández Y, Zubizarreta L, Calvo EG, Bermúdez JM. Microwave heating processes involving carbon materials. Fuel Process Technol 2010;91:1-8.

[18] Pruna A, Pullini D, Busquets D. Influence of synthesis conditions on properties of green-reduced graphene oxide. J Nanopart Res 2013:15:1605.

[19] Becerril HA, Mao J, Liu Z, Stoltenberg RM, Bao Z, Chen Y. Evaluation of solution-processed reduced graphene oxide films as transparent conductors. ACS Nano 2008;2(3):463-470.

[20] Benavente R, Borrell A, Salvador MD, García-Moreno O, Peñaranda-Foix FL, Catalá-Civera JM. Fabrication of near-zero thermal expansion of fully dense β-eucryptite ceramics by microwave sintering. Ceram Int 2014;40:935-941.

[21] Oliver WC, Pharr GM. An improved technique for determining hardness and elastic modulus using load and displacement sensing indentation experiments. J Mater Res 1992;7:1564-83.

[22] Mei XG, Ouyang JY. Ultrasonication-assisted ultrafast reduction of

graphene oxide by zinc powder at room temperature. Carbon 2011;49:5389-5397.

[23] Li J, Liu CY. Ag/Graphene heterostructures: synthesis, characterization and optical properties. Eur J Inorg Chem 2010;8:1244-1248.

[24] Jeong HK, Lee YP, Lahaye RJWE, Park MH, An KH, Kim IJ, Yang CW, Park CY, Ruoff RS, Lee YH. Evidence of graphitic AB stacking order of graphite oxides. J Am Chem Soc 2008;130:1362-1366.

[25] Wang SJ, Geng Y, Zheng Q, Kim JK. Fabrication of highly conducting and transparent graphene films. Carbon 2010;48:1815-1823.

[26] Kozak J, Rajurkar KP, Chandarada N. Machining of low electrical conductive materials by wire electrical discharge machining (WEDM). J Mater Process Technol 2004;149:266-71.

[27] Ho KH, Newman ST. State of the art electrical discharge machining (EDM). Int J Mach Tools Manuf 2003;43:1287-300.

[28] Malek O, González-Jesús J, Vleugels J, Vanderauwera W, Lauwers B, Belmonte M. Carbon nanofillers for machining insulating ceramics. Mater Today 2011;14:496-501.

[29] Zhu C, Guo S, Fang Y, Dong S. Reducing Sugar: New Functional Molecules for the Green Synthesis of Graphene Nanosheets. ACS Nano 2010;4(4):2429-2437.

[30] Kudin KN, Ozbas B, Schniep HC, Prud'homme RK, Aksay IA, Car R. Raman Spectra of Graphite Oxide and Functionalized Graphene Sheets. Nano Lett 2008;8:36.

[31] Ni ZH, Yu T, Lu YH, Wang YY, Feng YP, Shen ZX. Uniaxial strain on graphene: Raman spectroscopy study and band-gap opening. ACS Nano 2008, 2, 2301-2305.

[32] Elias DC, Nair RR, Mohiuddin TMG, Morozov SV, Blake P, Halsall MP, Ferrari AC, Boukhvalov DW, Katsnelson MI, Gein AK, Novoselov KS. Control of graphene's properties by reversible hydrogenation: evidence for graphene. Science 2009;23:610–613.

[33] Dai B, Fu L, Liao L, Nan Liu, Yan K, Chen Y, Liu Z. High-quality single-layer graphene via reparative reduction of graphene oxide. Nano Res 2011;4:434–439.

[34] Ni ZH, Wang HM, Ma Y, Kasim J, Wu YH, Shen ZX. Tunable stress and controlled thickness modification in graphene by annealing. ACS Nano 2008;2(5):1033–1039.

[35] Becerril HA, Mao J, Liu Z, Stoltenberg RM, Bao Z, Chen Y. Evaluation of solution-processed reduced graphene oxide films as transparent conductors. ACS Nano 2008;2:463-470.

[36] Coble L. Sintering crystalline solids. J Appl Phys 32 (1961) 787-793.

[37] Botero CA, Jiménez-Piqué E, Baudín C, Salán N, Llanes L. Nanoindentation of Al_2O_3/Al_2TiO_5 composites: Small-scale mechanical properties of Al_2TiO_5 as reinforcement phase. J Eur Ceram Soc 2012;32:3723-31.

[38] Botero CA, Jiménez-Piqué E, Seuba J, Kulkarni T, Sarin VK, Llanes L. Mechanical behaviour of $3Al_2O_3{\cdot}2SiO_2$ films under nanoindentation. Acta Mater 2012;60:5889-99.

Table 1. Carbon content, density and electrical resistivity of samples sintered at 1400 ºC by conventional (CS) and non-conventional (MW) methods for 120 min and 10 min, respectively.

Sintered samples	C content (wt.%)	Relative density (%)	Resistivity (Ω cm)
Al_2O_3-rGO/CS	1.65	92.2	1.3
Al_2O_3-rGO/MW	1.70	98.9	0.39

Table 2. Effect of sintering approach on the reduction of GO.

Material	v_D (cm^{-1})	v_G (cm^{-1})	I_D/I_G	I_{2D}/I_G
GO	1358	1598	0.76	0.42
Al_2O_3-rGO/MW	1352	1598	1.05	0.18
Al_2O_3-rGO/CS	1354	1584	0.62	1.5

Captions

Figure 1. FTIR spectra (a) and XRD patterns (b) of GO and graphite.

Figure 2. (a) TEM and (b) AFM images of GO.

Figure 3. (a) Raman spectra of GO before and after sintering procedure and (b) XRD spectra of the powders before and after sintering.

Figure 4. FE-SEM images of: (a) Al_2O_3 powder, (b) Al_2O_3-GO powder mix, (c) Al_2O_3 sintered by conventional method, (d) Al_2O_3-rGO sintered by conventional method and (e) Al_2O_3-rGO sintered by microwaves.

Figure 5. The change in the mechanical properties of Al_2O_3-rGO as a function of sintering approach: a) Young's modulus and b) hardness.

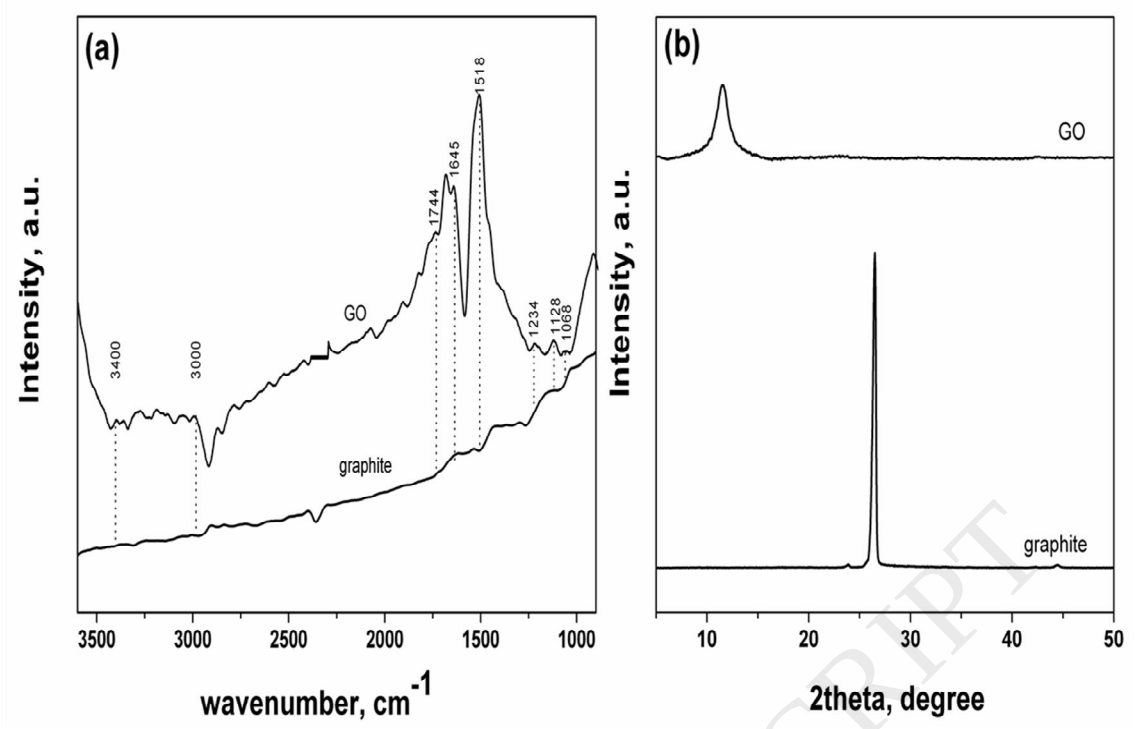

fig 1R .

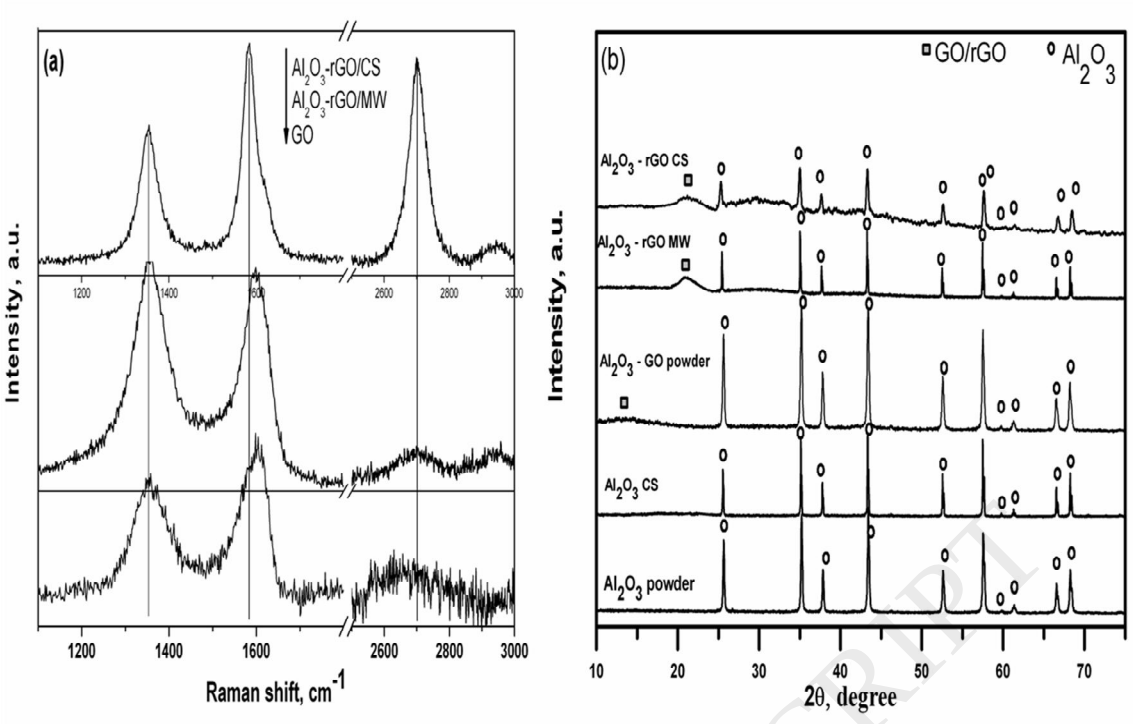

fig 3R .

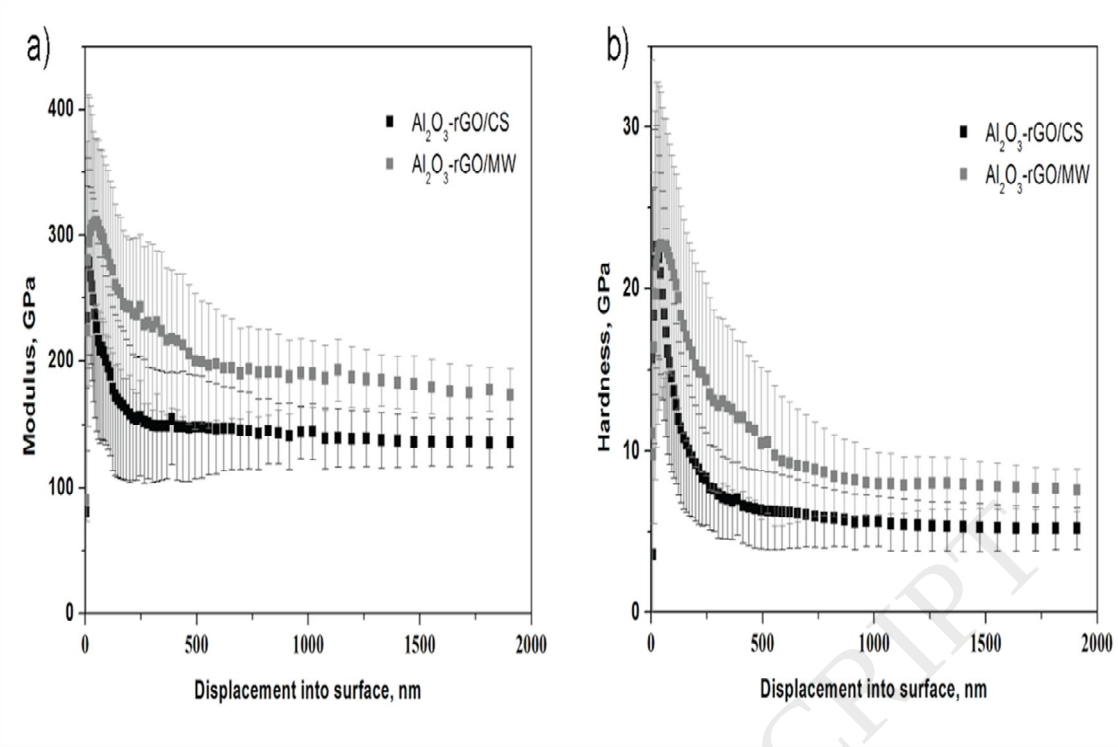

Fig 5 .

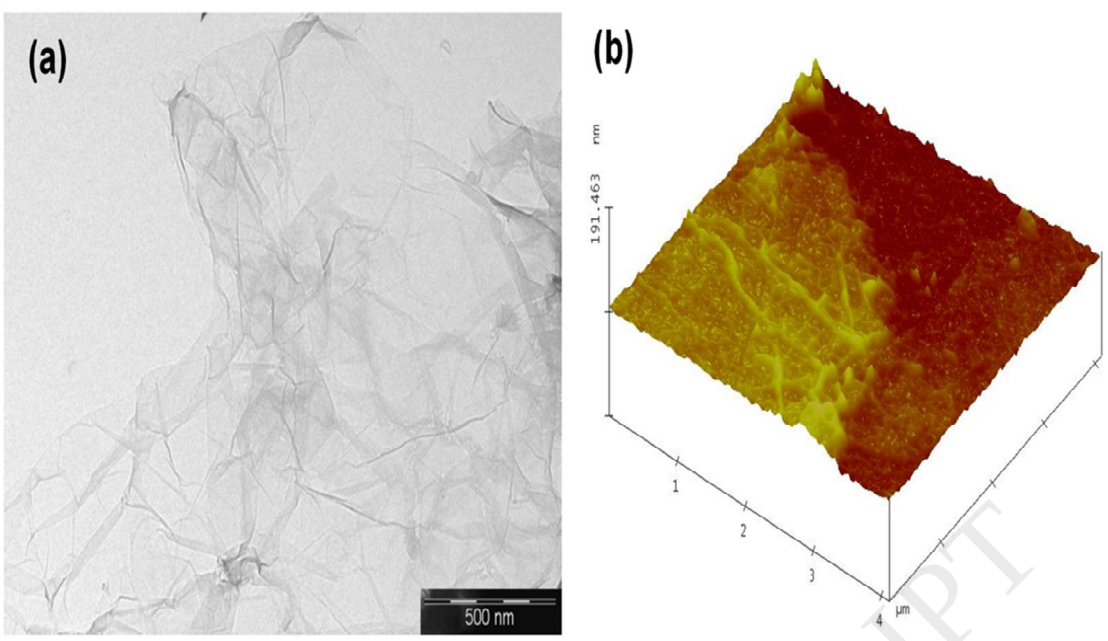

fig2_f .

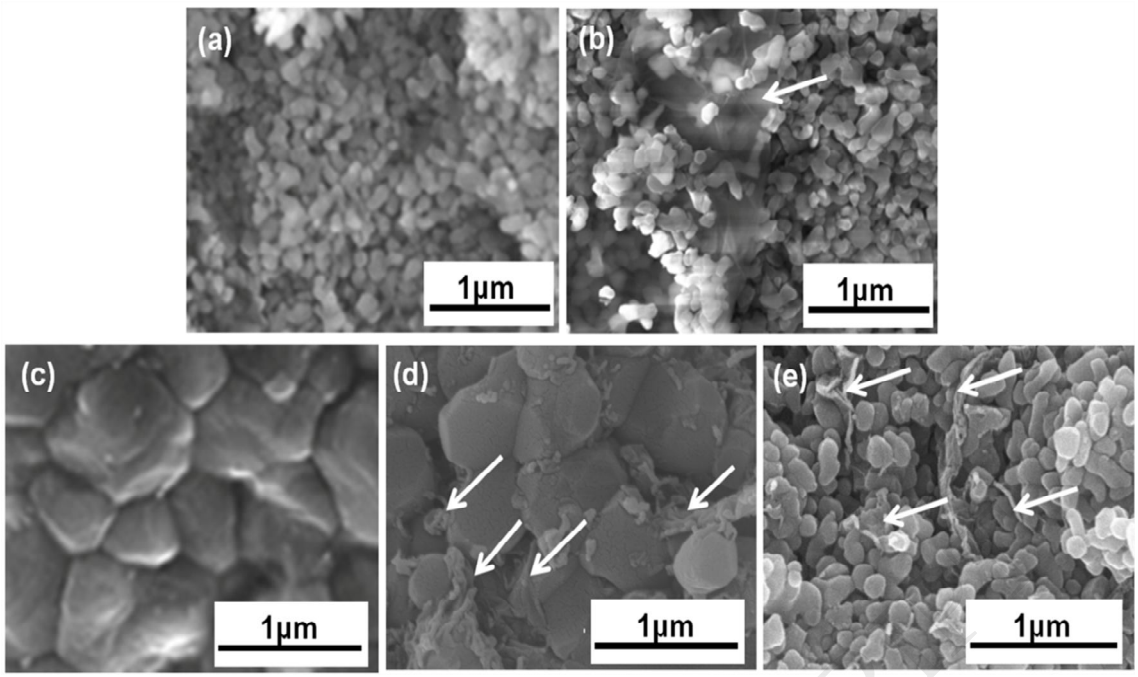

fig4R2 .